REPORT DOCUMENTATION PAGE

1

Form Approved OMB NO. 0704-0188

1. REPORT DATE (DD-MM-YYYY)	2. REPORT TYPE	3. DATES COVERED (From - To)
	New Reprint	-

4. TITLE AND SUBTITLE
Endogenous Bone Regeneration Is Dependent Upon a Dynamic Oxygen Event

5a. CONTRACT NUMBER
W911NF-09-1-0305

5b. GRANT NUMBER

5c. PROGRAM ELEMENT NUMBER
611103

6. AUTHORS
Mimi C Sammarco, Jennifer Simkin, Danielle Fassler, Alex J Cammack, Aaron Wilson, Keith Van Meter, Ken Muneoka

5d. PROJECT NUMBER

5e. TASK NUMBER

5f. WORK UNIT NUMBER

7. PERFORMING ORGANIZATION NAMES AND ADDRESSES
Tulane University
Administrators of the Tulane Educational Fund
6823 St. Charles Avenue
New Orleans, LA 70118 -5665

8. PERFORMING ORGANIZATION REPORT NUMBER

9. SPONSORING/MONITORING AGENCY NAME(S) AND ADDRESS (ES)
U.S. Army Research Office
P.O. Box 12211
Research Triangle Park, NC 27709-2211

10. SPONSOR/MONITOR'S ACRONYM(S)
ARO

11. SPONSOR/MONITOR'S REPORT NUMBER(S)
56157-LS-MUR.27

12. DISTRIBUTION AVAILIBILITY STATEMENT
Approved for public release; distribution is unlimited.

13. SUPPLEMENTARY NOTES
The views, opinions and/or findings contained in this report are those of the author(s) and should not contrued as an official Department of the Army position, policy or decision, unless so designated by other documentation.

14. ABSTRACT
Amputation of the digit tip within the terminal phalangeal bone of rodents, monkeys, and humans results in near-perfect regeneration of bone and surrounding tissues; however, amputations at a more proximal level fail to produce the same regenerative result. Digit regeneration is a coordinated multi-faceted process that incorporates signaling from bioactive growth factors both in the tissue matrix and from several different cell populations. To elucidate the mechanisms involved in bone regeneration we developed a novel multi-tissue slice culture model that regenerates bone ex vivo via direct ossification. Our study provides an integrated multi-tissue system for bone and digit

15. SUBJECT TERMS
Cell/Tissue Signaling - other, Bone QCT/?CT, Matrix mineralization, Molecular pathways -remodeling, Cells of bone – osteoblasts

16. SECURITY CLASSIFICATION OF:			17. LIMITATION OF ABSTRACT	15. NUMBER OF PAGES	19a. NAME OF RESPONSIBLE PERSON
a. REPORT	b. ABSTRACT	c. THIS PAGE			Ken Muneoka
UU	UU	UU	UU		19b. TELEPHONE NUMBER: 504-865-5059

Standard Form 298 (Rev 8/98)
Prescribed by ANSI Std. Z39.18

Report Title

Endogenous Bone Regeneration Is Dependent Upon a Dynamic Oxygen Event

ABSTRACT

Amputation of the digit tip within the terminal phalangeal bone of rodents, monkeys, and humans results in near-perfect regeneration of bone and surrounding tissues; however, amputations at a more proximal level fail to produce the same regenerative result. Digit regeneration is a coordinated multi-faceted process that incorporates signaling from bioactive growth factors both in the tissue matrix and from several different cell populations. To elucidate the mechanisms involved in bone regeneration we developed a novel multi-tissue slice culture model that regenerates bone ex vivo via direct ossification. Our study provides an integrated multi-tissue system for bone and digit regeneration and allows us to circumvent experimental limitations that exist in vivo. We utilized this slice culture model to evaluate the influence of oxygen on regenerating bone. Micro-computed tomography (?CT) and histological analysis revealed that the regenerative response of the digit is facilitated in part by a dynamic oxygen event, where mutually exclusive high and low oxygen micro-environments exist and vacillate in a coordinated fashion during regeneration. Areas of increased oxygen are initially seen in the marrow and then surrounding areas of vasculature in the regenerating digit. Major hypoxic events are seen at 7 days post-amputation (DPA) in the marrow and again at DPA 12 in the blastema, and manipulation of oxygen tensions during these hypoxic phases can shift the dynamics of digit regeneration. Oxygen increased to 21% oxygen tension can either accelerate or attenuate bone mineralization in a stage-specific manner in the regenerative timeline. These studies not only reveal a circumscribed frame of oxygen influence during bone regeneration, but also suggest that oxygen may be one of the primary signaling influences during regeneration.

REPORT DOCUMENTATION PAGE (SF298)
(Continuation Sheet)

Continuation for Block 13

ARO Report Number 56157.27-LS-MUR
Endogenous Bone Regeneration Is Dependent l...

Block 13: Supplementary Note

Approved for public release; distribution is unlimited.

Original Article

Endogenous Bone Regeneration Is Dependent Upon a Dynamic Oxygen Event**

Mimi C Sammarco (co-first), PhD †[1], Jennifer Simkin (co-first), BS †[1], Danielle Fassler, BS[2], Alex J Cammack[1], Aaron Wilson[3], Keith Van Meter, MD[4], and Ken Muneoka, PhD[1]*

[1] Tulane University, Department of Cell and Molecular Biology, 6400 Freret St, 2000 Percival Stern Hall, New Orleans, LA 70118, Phone: 504-865-5546, Fax: 504-865-6785
Ken Muneoka, kmuneoka@tulane.edu, DARPA-W911NF-06-1-0161, ARO-W911NF0910305, and the John L. and Mary Wright Ebaugh Endowment Fund at Tulane University.
Mimi Sammarco, msammarc@tulane.edu, Eunice Kennedy Shriver National Institute of Child Health and Human Development NIH-F32HD071763-02, Musculoskeletal Transplant Foundation Junior Investigator Grant 2012
Jennifer Simkin, jsimkin2@tulane.edu
Alex Cammack, acammack@tulane.edu

[2] Stony Brook University Medical Center, School of Medicine, Basic Science Tower, Floor T-8/Room 101, Stony Brook, NY, 11794, Phone: 631-444-3219, Fax: 631-444-3492
Danielle Fassler, dfassler2@gmail.com

[3] Baromedical Research Institute, Ocean Advanced Research, 1816 Industrial Blvd, Harvey, LA, 70058, Phone: 504-366-1445
Aaron Wilson, wilsonA06@yahoo.com

[4] Louisiana State University Health Sciences Center, Department of Medicine, 2021 Perdido St, New Orleans, LA,70112, Phone: 504-903-3594, Fax: 504-903-4569
Keith Van Meter, kvanme@lsuhsc.edu

* Corresponding author: kmuneoka@tulane.edu or 504-865-5059

† First author

Disclosures: All authors state that they have no conflicts of interest. The funders had no role in study design, data collection and analysis, decision to publish, or preparation of manuscript.

Additional Supporting Information may be found in the online version of this article.

Initial Date Submitted December 2, 2013; Date Revision Submitted March 17, 2014; Date Final Disposition Set March 31, 2014

DOI 10.1002/jbmr.2261

Abstract

Amputation of the digit tip within the terminal phalangeal bone of rodents, monkeys, and humans results in near-perfect regeneration of bone and surrounding tissues; however, amputations at a more proximal level fail to produce the same regenerative result. Digit regeneration is a coordinated multi-faceted process that incorporates signaling from bioactive growth factors both in the tissue matrix and from several different cell populations. To elucidate the mechanisms involved in bone regeneration we developed a novel multi-tissue slice culture model that regenerates bone *ex vivo* via direct ossification. Our study provides an integrated multi-tissue system for bone and digit regeneration and allows us to circumvent experimental limitations that exist *in vivo*. We utilized this slice culture model to evaluate the influence of oxygen on regenerating bone. Micro-computed tomography (μCT) and histological analysis revealed that the regenerative response of the digit is facilitated in part by a dynamic oxygen event, where mutually exclusive high and low oxygen micro-environments exist and vacillate in a coordinated fashion during regeneration. Areas of increased oxygen are initially seen in the marrow and then surrounding areas of vasculature in the regenerating digit. Major hypoxic events are seen at 7 days post-amputation (DPA) in the marrow and again at DPA 12 in the blastema, and manipulation of oxygen tensions during these hypoxic phases can shift the dynamics of digit regeneration. Oxygen increased to 21% oxygen tension can either accelerate or attenuate bone mineralization in a stage-specific manner in the regenerative timeline. These studies not only reveal a circumscribed frame of oxygen influence during bone regeneration, but also suggest that oxygen may be one of the primary signaling influences during regeneration.

Key Words: Cell/Tissue Signaling - other, Bone QCT/μCT, Matrix mineralization, Molecular pathways - remodeling, Cells of bone - osteoblasts

Introduction

Oxygen has been implicated in almost every mechanism of multicellular existence and is readily diffusible across cell membranes, necessitating a complex system to maintain cellular and organismal oxygen homeostasis. It is hard to overstate the significance of oxygen in wound healing and regeneration; however, the ability to both control and measure oxygen tension *in vivo* presents an impediment to investigating oxygen at a cellular level. As a result, little is known regarding the influence of oxygen during complex processes like regeneration.

Digit tip regeneration is a well-characterized series of phases [1-3] that provides a predictable model in which to study environmental influences such as oxygen. After amputation, the terminal phalangeal element (P3) in humans [4-7], primates, and mice regenerates [2, 8]. The regenerative process occurs regardless of age in both mice [3, 8-10] and humans [11-13]. Digit regeneration in adult mice, after the growth plate has completed ossifying and the terminal phalangeal element has reached maximal length [1, 8], follows a defined sequence of phases (or stages) including a bone degradation and epidermal closure phase (7 to 12 days post-amputation, DPA 7-12), a blastema formation phase (DPA 12), and a blastema differentiation phase (DPA 14 and later) in which the bone and surrounding connective tissue is reformed [1, 2]. *In vivo* the mouse digit tip regeneration culminates in woven cancellous bone that does not completely remodel into cortical bone, even after 128 days [2, 5]. The mouse digit blastema is a temporary structure composed of undifferentiated, proliferating cells which express developmentally relevant genes [1, 2] similar to the regenerating limbs of salamanders and is central to the regenerative process [1, 2, 14-16]. The digit blastema shows reduced vascularity [2, 16], and precedes the intramembranous formation of bone, which is largely linked to angiogenic events in skeletal development [17, 18]. While the vascular profiles suggest a changing oxygen microenvironment during digit regeneration, actual oxygen tensions during regeneration have yet to be shown. Furthermore, reactive oxygen species (ROS) have been shown to be integral for Xenopus [19] and zebrafish [20] regeneration and are consistent with the idea that oxygen has a specific role in mammalian regeneration.

Oxygen is also essential for successful wound healing, and has been the focus of many studies. Tissue oxygen availability in the wound provides a basic biochemical energy supply and is necessary for the generation of

ROS to protect the site against bacterial infection [21, 22], for collagen synthesis [23], which ultimately determines the strength of the newly fabricated tissue, and for epithelialization [24]. On the other hand, hypoxia in acute wounds serves as an impetus for angiogenesis [25] and initiates the early stages of wound healing via ROS initiated cellular signaling [26, 27]. The seemingly contradictory nature of oxygen's effect on cell activity can be difficult to unravel *in vivo*.

In vitro experiments can offer some insight into oxygen's influence on cells. However, most *in vitro* approaches are limited by the lack of relevant structures. To overcome this limitation, we employ a multi-tissue slice culture technique. Slice culture is an *ex vivo* technique predominantly used to evaluate neuronal connectivity, since it maintains the integrity of the neuronal architecture [28]. Building upon this technique, one group established a slice culture model of rat incisor teeth to study dentinogenesis, which requires contact between odontoblasts and the dentine matrix to maintain phenotypic morphology, secretory activity, and cell-cell and cell-matrix interactions [29]. Similarly, subsequent studies were able to culture explanted calvarial bones to better understand bone growth [30] and underlying mesenchymal interactions [31]. Thus, the slice culture model offers better control over experimental variables such as oxygen while maintaining the structural integrity of a bone regenerating environment.

In this study we create and characterize a slice culture model of the P3 digit regenerative process and use the model to investigate the influence of oxygen on bone regeneration. We show that P3 digit regeneration exhibits temporally specific responses to changing oxygen tensions both *ex vivo* and *in vivo*. High oxygen applied during P3 bone degradation exacerbates and prolongs the degradation phase. Increased oxygen tension applied during the blastema phase attenuates bone formation. Finally, high oxygen applied during bone formation accelerates bone formation when compared to hypoxic conditions. Our study identifies temporally specific oxygen events during P3 regeneration that, once mechanistically dissected, will offer a clinical point of intervention for future treatments.

Materials and Methods

Amputations and animal handling

Adult 8-week old [1, 8] female CD1 mice were obtained from Charles River Laboratories (Wilmington, MA). Mice were anesthetized with 1-5% isoflurane gas with continuous inhalation. The second and fourth digits of one hind limb were amputated at the P3 distal level as described previously [2] and regenerating digits were collected at designated times for slice culture. The third digit was used as an unamputated control. All experiments were performed in accordance with the standard operating procedures approved by the Institutional Animal Care and Use Committee of Tulane University Health Sciences Center.

Slice and explant culture

At the designated day post-amputation, mice were euthanized and sterilized with iodine before removing the second, third and fourth digits from the hind limb and placing in ice-cold media (20% FBS, 60% high glucose DMEM, 40% HBSS). Digits were glued to the sample platform with the lateral plane parallel to the direction of motion of the vibratome blade. 250 μm sections were made with a Leica VT1200 vibratome (Leica, Buffalo Grove, IL) such that the marrow cavity of P3 was not compromised by the blade, removing most epithelium and connective tissue from each side of the digit. Slices were then placed in iced media and embedded in Extracel hydrogel (Glycosan, Salt Lake City, UT) in a 8.0 μm PET track-etched trans-well (Falcon, Franklin Lakes, NJ). For blastema explants, DPA 12 mice were euthanized and blastemas were surgically removed on ice before being embedded in hydrogel. Samples were maintained at 37°C in either 1% oxygen (5% CO_2, balance N_2) or standard tissue culture conditions (21% oxygen and 5% CO_2); media was changed every two days. Micro-CT imaging was utilized for consistency of regenerative staging in the slice samples, DPA 14 samples included only those that were beginning to form active bone, and DPA 12 samples included only those that had not yet begun to show new bone formation.

Tissue collection and histology

Digits were fixed overnight in zinc-buffered formalin (Z-fix, Anatech, Battle Creek, MI). Bone was decalcified for 8 hours in a formic-acid based decalcifier (Decal I, Surgipath, Richmond, IL). Once decalcified, all samples were

processed for paraffin embedding using a Leica TP 1020 Processor (Leica, Buffalo Grove, IL). For the evaluation of cell proliferation, the Click-iT EdU cell proliferation assay (Invitrogen, Carlsbad, CA), based on an analogue of bromodeoxiuridine: EdU (5-ethynyl-2'-deoxyuridine), was used according to the manufacturer's protocol. Click-iT TUNEL assays (Invitrogen, Carlsbad, CA) were performed according to the manufacturer's protocol. Fluorescent photomicrographs were captured using an Olympus BX61 deconvolution microscope (Olympus America Inc, Center Valley, PA). Serial sections were stained with Mayer's hematoxylin and Eosin Y (Sigma-Aldrich, St. Louis, MO) and mounted using permanent mounting medium (Fisher Scientific, Waltham, MA). Whole mount bone was visualized with an Alizarin red stain as described previously [(1)]. Brightfield micrographs were captured using an Olympus DP72 camera mounted on an Olympus BX60 microscope (Olympus America Inc, Center Valley, PA) and whole mount images were captured using a Zeiss Axiocam mounted on a Zeiss Stereoscope (Carl Zeiss, Oberkochen, Germany). Final figures were generated using Adobe Photoshop CS4.

Fluorescent immunohistochemistry and quantification of oxygen signal

Immunofluorescent staining was performed on deparaffinized and rehydrated sections with specific primary antibodies: osterix (rabbit anti-mouse; Abcam ab22552, Cambridge, MA), hypoxyprobe™-1 Plus (Hypoxyprobe, Burlington, MA) and FBXL5 (rabbit anti-mouse, Abcam ab102692, Cambridge, MA). Primary signal was amplified with either Alexa Fluor secondary antibodies (Invitrogen, Carlsbad, CA) or a tyramide signal amplification kit (Invitrogen, Carlsbad, CA) per manufacturer's instructions. Calcein green was administered to mice via intraperitoneal injection (20 mg/kg) (Sigma-Aldrich, St. Louis, MO) at DPA 13 and digits were harvested 24 hours later at DPA 14. Calcein-positive slices were subsequently cultured in 1 μg/mL Alizarian Complexone (Sigma-Aldrich, St. Louis, MO) in culture media in standard tissue culture conditions, protected from light. Samples were incubated in 0.3 M sucrose at 37° C for 4 hours, snap frozen, cryosectioned and analyzed for bone formation using a fluorescent deconvolution microscope. Administration of hypoxyprobe™-1 Plus was per the manufacturer's instructions. Briefly, hypoxyprobe™-1 Plus was administered via intraperitoneal injection at a dosage of 60 mg/kg. Mice were sacrificed and digits harvested and fixed in Z-fix after 45 minutes. To quantitatively determine the total area of positive signal, photomicrographs of entire representative digit sections were obtained at 40x using an Olympus BX61 fluorescent deconvolution microscope (Olympus America Inc,

Center Valley, PA). Quantification of osterix, hypoxyprobe, FBXL5, or DAPI + area was performed on 4 separate samples per time point by thresholding fluorescent signal and masking subsampling with Slidebook Imaging software (Intelligent Imaging Innovations, Denver CO). The ratio of total osterix, hypoxyprobe or FBXL5 + area per total DAPI + area was then calculated.

Micro-computed tomography (μCT)

Micro-CT images were acquired using a VivaCT 40 (Scanco Medical AG, Brüttisellen, Switzerland) at 1000 projections per 180 degrees with a voxel resolution of 10 μm^3, and energy and intensity settings of 55 kV and 145 μA. Integration time for capturing the projections was set to 380 ms using continuous rotation. Images were segmented using the BoneJ [32] (Version 1.2.1) Optimize Threshold Plugin for ImageJ (Version1.48c). Changes in bone volume were quantified using the BoneJ Volume Fraction Plugin for ImageJ and bone volume was normalized to total bone volume at DPA 0. Changes in bone thickness were mapped using the Trabecular Thickness Plugin for ImageJ and 3D renderings of the μCT scans and the bone thickness maps were created using the 3D viewer plugin for ImageJ.

Hyperbaric Oxygen Treatment (HBOT)

Mice were randomly assigned to receive HBOT at DPA 11 and DPA 13. The control group did not receive HBOT. Mice were placed in the hyperbaric chamber (Baromedical Research Institute - Van Meter and Assoc., Harvey, LA) and received 90 min of 100% oxygen at 2.4 atmospheres absolute (ATA). Compression and decompression of the chamber were executed at 2 psi/minute.

Statistical analysis

Statistically significant differences were determined using unpaired t-tests with one-or two-tailed distributions using KaleidaGraph (Version 4.1.1, Synergy Software, Reading, PA). A value of $p<0.05$ was deemed statistically significant. In all cases, data are represented as mean ± standard error of mean (SEM).

Results

Digit regeneration is associated with a dynamic oxygen profile

P3 digit regeneration is a dynamic process that involves specific phases including inflammation, re-epithelialization, bone degradation, blastema formation, and soft tissue and bone regeneration. The bone-specific

stages can be seen in the μCT renderings of Figure 1. Following amputation, the bone volume of the remaining P3 decreases to an average of 68% of the volume at amputation (DPA 0) and begins to rise again around DPA 12-14 (Fig. 1A). 3D renderings of μCT scans demonstrate the phases of bone degradation and regeneration (Fig. 1B). At the point where change in bone volume begins to turn around (DPA 12-14), analysis of osterix, a nuclear-localized early marker of osteoblast differentiation [33], shows that there are almost 10% more osterix-positive cells at DPA 14 than at DPA 12 ($p=0.037$) (Fig. Suppl. 1), whereas staining for cell proliferation suggests that the number of dividing cells remains statistically indistinguishable between these two time points (Fig. Suppl. 1).

To determine whether the oxygen microenvironment of the P3 regenerating digit is a dynamic variable, we evaluated hypoxic oxygen events *in vivo* using the reductive 2-nitroimidazole compound pimonidazole Hypoxyprobe-1 (Hypoxyprobe), which forms stable adducts in hypoxic areas (<1.3% oxygen) that are identified using an anti-pimonidazole antibody [34-36]. This analysis included unamputated digits as well as regenerating digits collected at DPA 0, 3, 7, 10, 12, 14, and 21. The unamputated digit demonstrates minimal area that is less than 1.3% oxygen (Fig. 2A). Hypoxic areas at DPA 0, shortly after amputation, are limited to the epithelium and scattered cells within the marrow (Fig 2B). At DPA 3, positive hypoxic signal is slightly increased in the marrow area and endosteum of the bone, and in the nail epidermis, particularly in the stratum basale (Fig. 2C). DPA 7 shows extensive hypoxic signal within the marrow cavity (Fig. 2D), affiliated with cuboidal bone lining cells (Fig. Suppl. 2A and B) and associated with osteoclasts on the ejecting bone (Fig. Suppl. 2C). By DPA 10, hypoxic signal is associated with the endosteum and the junction between the remaining distal bone stump and the forming blastema (Fig. 2E). Interestingly, hypoxic signal is less robust at DPA 10 than at DPA 7, and is predominantly affiliated with the lining of the distal edge of the bone stump (Fig. 2E, arrow). By DPA 12, the majority of the newly forming bone, blastema area, and endosteum are hypoxic, and hypoxyprobe signal in the nail epithelium has expanded to include the distal area of the nail bed (Fig. 2F). As bone continues to form at DPA 14 hypoxic signal localizes to the osteoblasts at the perimeter of the newly forming trabecular bone, and can also be detected in the marrow space, endosteum and nail epithelium (Fig. 2G). By DPA 21 hypoxyprobe signaling is still apparent in osteoblasts in the newly formed trabecular bone, but to a lesser extent than that seen in DPA 14 (Fig. 2H).

In order to confirm hypoxic events and evaluate endogenous events of increased oxygen, we analyzed the expression of F-box and leucine-rich repeat protein 5 (FBXL5). FBXL5 is critical to maintaining iron homeostasis within the cell. The protein is degraded in hypoxic conditions [37-39] as part of an inverse response to HIF-1α stabilization, which begins at 6% oxygen and increases exponentially as oxygen continues to decrease [40]. FBXL5 stabilization above 6% oxygen tension is independent of iron concentrations [41-43]. FBXL5 signal in the unamputated digit is restricted to the P3 marrow cavity (Fig. 2A'). This signal within the marrow expands after amputation to include the mesenchymal tissue dorso-proximal to the nail and the endosteum of P3 (Fig. 2B'). At DPA 3 FBXL5 signal is sustained in the marrow and in the nail matrix, in a pattern that expands towards the amputated tip (Fig. 2C'). This pattern continues through DPA 7 (Fig. 2D'). By DPA 10, FBXL5 signal is evident in the newly forming soft tissue immediately distal to the bone stump, extending towards the distal tip of P3, and affiliated with vasculature within the marrow (Fig. 2E'). As P3 regeneration begins with the new formation of bone at DPA 12, FBXL5 signal is apparent on the dorsal side and distal tip of P3, as well as within the marrow (Fig. 2F'). By DPA 14 FBXL5 signal has extended completely down the dorsal side of P3 towards the distal tip affiliated with cells that surround the vascular lumen (Fig. 2G'). This signal within the distal tip of P3 expands at DPA 21, associated predominantly with new vasculature and with the area at the proximal base of the dorsal P3 connective tissue (Fig. 2H').

These two profiles, taken together show mutually exclusive patterning of areas representative of less than 1.3% oxygen, and above 6% oxygen, and demonstrate that there are multiple oxygen micro-environments within the regenerating P3 digit. The blastema phase, which occurs between DPA 10 and 14, appears to be the most dynamic of the temporal oxygen changes. To more closely evaluate oxygen levels, we quantified the areas of hypoxyprobe and FBXL5 fluorescent signals independently as a function of overall DAPI signal in the P3 area (see materials and methods) (Fig. 2I-L). Quantification of the oxygen profiles during this time period, where the absence of either probe is defined as normoxic in our digit model, shows that there is no significant change in overall amount of FBXL5 signal during these three time points. Conversely, hypoxic area is lowest at DPA 10 (11%) but shows a significant increase to 48% ($p=0.019$) during DPA 12. At DPA 14, the area of hypoxia drops slightly to 37%, although this number is not significantly different from DPA 12 ($p=0.506$). The percentage of

normoxic cells over time decreases as the number of hypoxic cells increases and the number of FBXL5-positive cells remains the same.

Explant slice culture model exhibits temporally specific bone growth

The oxygen profile of P3 supports a dynamic oxygen microenvironment during regeneration. We hypothesized that increasing oxygen at specific time points during P3 regeneration would either attenuate or enhance the individual phases of P3 regeneration. In order to control oxygen tension during P3 regeneration, we engineered an ex vivo slice culture digit explant model of P3. The regenerating P3 mouse digit was removed at DPA 0, 3, 7, 11, or 14 (Suppl. 3 A and B, Fig. 3A-C,) and a 250 μm median sagittal section was taken without exposing the marrow; the nail, epithelium and underlying connective tissue was removed from each side to increase oxygen and nutrient availability. We compared regeneration in slice explants after 7 days in culture (7 days post slice, DPS 7) (Fig. 3D-F) to regeneration after 7 days in vivo (Fig. 3G-I). Digit slices were cultured at 21% oxygen and 5% CO_2. Bone formation was assessed using Alizarin red staining. Bone morphology is shown for 1) 24 hours of slice culture (initial time) (Fig. 3A-C), 2) after 7 days of slice culture (Fig. 3D-F), and 3) for comparable bone regeneration, after 7 days in vivo (Fig. 3G-I). Explant cultures that represent DPA 0 and 3 show little change in bone morphology ex vivo and minimal degradation (Fig. Suppl. 3A-F), while slice culture samples from DPA 7, when P3 is actively degrading bone in vivo (Fig. 3A), continue to actively degrade bone ex vivo (Fig. 3D). DPA 11 samples, which represent the hypoxic blastema stage (Fig. 3B), show minimal progression of bone growth (Fig. 3E). Similarly, DPA 14 samples, taken when P3 is actively regenerating bone, show bone growth with no evidence of cartilage formation (Fig. 3C and F). Based on our timed explant studies, P3 slice regeneration is restricted to DPA 14 (active bone growth stage) and to a lesser degree to DPA 11 (blastema stage) and occurs at the distal tip of the P3 stump (Fig. 3E and F).

Dynamic labeling of newly formed bone *in vivo* at DPA 13 with calcein green prior to generating slice samples (DPA 13), followed by incubation in culture with alizarin complexone shows that bone forms in slice culture *ex vivo* (Fig. 3J-K). *In vivo* (green) and *ex vivo* (red) bone formation are mutually exclusive, and areas of *ex vivo* bone growth occurs both on trabeculae of bone previously formed *in vivo* (red bone around green center, Fig.

3J arrow) and in *de novo* trabeculae (red islands without green center, Fig. 3J asterisk). By DPS 6, osterix-positive cells are evident in close proximity to areas of *ex vivo* bone formation at the distal tip of P3, (Fig. 3K,asterisk). In contrast, osterix-negative cells are found in close proximity to areas of calcein-positive bone previously deposited *in vivo* (Fig. 3K arrow).

Increased oxygen effects bone mineralization in DPA 14, but not DPA 12 slice explant cultures

To better understand the influence of oxygen on our explants, we characterized the DPA 14 slice explants in 21% O_2 and quantified bone regeneration. Digit slices were cultured for two weeks, and bone volume changes were quantified using μCT at DPS 0, 7, and 14. An overlay of μCT images shows bone growth from 0 days in culture to 14 days in culture (Fig. 4A). Micro-CT trabecular thickness (Tb.Th) analysis of the slice samples shows that bone regeneration and remodeling occurs predominantly in, but is not restricted to, the area directly adjacent to the P3 bone stump, and the dorsal and ventral areas flanking the bone stump (Fig. 4B). New bone forms at the distal edge of the original bone and Tb.Th of the new bone increases over time as trabecular spaces and cellular gaps between mineralized islands of bone consolidate through bone mineralization (Fig. 4B). Cross-sections of the newly formed bone show a defined marrow cavity perimeter throughout culture. Color-coding shows areas of transition as trabecular spacing decreases over time (Fig. 4B). New bone growth is completely restricted to the regenerating digit tip and does not occur anywhere else on the explanted slice (e.g. the proximal end of P3, within the joint or marrow cavity, or on the P2 bone (Fig. Suppl. 4).

Analysis of slice culture explant samples using terminal deoxynucleotidyl transferase (TdT)-mediated deoxyuridine triphosphate (dUTP)-biotin nick end-labeling (TUNEL) as an indicator of apoptotic [44, 45] and necrotic [46] cells, and Click-iT EdU Alexa Fluor Imaging Assay (Invitrogen) to label proliferating cells, show a non-proliferating, viable population of cells that persist throughout the experimental timeline (DPS 14) and beyond (DPS 21) (Fig. Suppl. 5). Further evaluation of the slice using osterix (OSX) shows that osterix positive cells can still be seen in the trabecular bone spaces, distal to the growing P3 bone stump, and within the tissue lining the bone at DPS 3 through DPS 12 (Fig. Suppl. 6A, B). This expression is consistent with formation of osteoid matrix

deposition between already mineralized trabeculae (Fig. Suppl. 6C, D). Collectively these data demonstrate that slice culture samples maintain a population of osteoblasts and continue to show bone mineralization.

Based on our findings that slice explants are viable and able to grow bone in culture, we used this model to test the effects of oxygen tensions on bone regeneration. We define specific oxygen micro-environments during regeneration that are consistent with the known *in vivo* range of <1% to 6% in bone marrow and surrounding tissue [47]. Thus a standard tissue culture environment of 21% oxygen represents an excessively high oxygen tension. DPA 14 slices show a significant increase in bone volume during a two week culture period at 21% oxygen (20%, p=0.0008; Fig. 4C) whereas DPA 12 slices show no significant change (p=0.584) in bone volume (Fig. 4D). This suggests that bone mineralization during digit regeneration is promoted by enhanced oxygen levels, but that this effect is stage dependent. In contrast, DPA 12 slice samples show a significant increase in bone volume when cultured in hypoxic conditions (1% oxygen) for two weeks (9%, p=0.007; Fig. 4D), whereas DPA 14 slice explants cultured in 1% oxygen attenuated the robust growth seen at 21% oxygen (5% increase, p=0.029; Fig. 4C). Together, these data suggest the existence of a transition in oxygen sensitivity that accompanies the shift during regeneration from a blastema stage to the re-differentiation stage.

A hypoxic event is integral to optimal bone regeneration

Hyperbaric oxygen treatment (HBOT) is a method of administering 100% oxygen at an increased atmospheric pressure. As a result, oxygen is able to saturate the plasma and hemoglobin alike, leading to elevated tissue oxygen tension [48]. Based on our data that a premature increase in oxygen at DPA 12 can attenuate bone regeneration *ex vivo*, we hypothesized that a similar interruption *in vivo* compromises P3 regeneration. To administer HBOT we utilized a specialized hyperbaric chamber to increase oxygen tension in mice *in vivo* at DPA 11 after P3 amputation. The use of hypoxyprobe in DPA 12 mice shows that hypoxic signal is abolished after a single 90 minute treatment of 100% oxygen at 2.4 atmospheres of pressure (ATA) (Fig. 5B) when compared to a control DPA 12 (Fig. 5A). Mice were subjected to two independent treatments of hyperbaric oxygen at DPA 11 and again at DPA 13, when hypoxic conditions are maximal, in order to disrupt the hypoxic event. Bone growth was based on bone volume measurements derived from μCT analyses and is analyzed as a percentage of the

amputated bone volume at DPA 0. An analysis of control digit bone volume (n=32) displays a consistent pattern of bone volume changes that include a regression period followed by a period of new bone growth (Fig. 1A and B, 5C and D). We note that while the overall pattern is consistent there is considerable variability between digits in the timing and extent of the bone regression phase, which is maximal at DPA 10 (Fig 1A), as well as the rate of new bone growth during the re-differentiation phase. The control response is divided into two groups. The first group (Fig. 5C) transitions from bone loss to bone gain between DPA 7 and DPA 10 (65% of digits tested). The second group (Fig. 5D) transitions from bone loss to bone gain between DPA 10 and DPA 14 (35% of digits tested). No digits show a transition from bone loss to bone gain later than DPA 14 (Fig 1A).

An analysis of HBOT treated digits (n=32) shows that regeneration itself is not inhibited and the overall pattern of bone loss and bone gain is not modified, but there is considerably more variability in the timing and extent of the bone regression phase (Fig. 5 E-F). This effect is most striking in a subset of digits (N=19, Fig. 5F) in which the bone regression phase extended to DPA 21 and was associated with bone loss. In this study we found a set of digits (Fig. 5E) that display a volume profile similar to control digits (Fig. 1A and 5C) where the samples transition from bone loss to bone gain between DPA 7 and DPA 10. When both the affected and unaffected digit sets are analyzed we are drawn to the general conclusion that if a digit is in a bone regression phase at the time of HBOT treatment, then the regression phase is extended, however if a digit has entered the blastema differentiation phase it is refractory to HBOT treatment. 3D renderings of a representative sample of the μCT data shown as a time lapse movie underscore the prolonged time period of degradation and reduced rate of regeneration (Movie. 5H) when compared to time-matched control digits (Movie. 5G) or HBOT treated digits that are refractory to oxygen. Note that the effects of the applied HBOT extend past the applied hyperbaric treatments. In addition, unamputated digits showed no evidence of accelerated bone turnover (data not shown). These HBOT findings parallel our oxygen profile of digit regeneration as well as our *ex vivo* slice explant data and implies that digit regeneration may involve a key transition in oxygen sensitivity that is associated with optimal bone regeneration.

Discussion

Mouse digit tip regeneration is unique in that it provides a predictable intramembranous bone regenerative response where outgrowth after amputation is from a defined region and occurs without exogenous induction. This makes P3 amputation an excellent model in which to study the effects of oxygen during regeneration. That oxygen tensions fluctuate during the P3 regeneration process is evident *in vivo* when viewing specific markers for hypoxia and hyperoxia, and our observation that P3 regeneration is associated with a mutable oxygen microenvironment is, to our knowledge, the first characterization of oxygen environments within a regenerating mammalian system. Areas of hypoxia and hyperoxia are temporally and spatially distinct and predictable. Within our described time frame, we observe two major hypoxic events: the first is within the bone marrow prior to blastema formation, and the second is associated with the regeneration blastema itself. In contrast, hyperoxic regions remain relatively constant during the regenerative response and are associated with the vasculature. Our *in vitro* and *in vivo* studies focusing on the blastema-specific hypoxic stage provide evidence that oxygen plays an active role in regulating the regeneration timeline and controls the normal transition from a bone degradation phase to a bone mineralization phase.

Hyperbaric oxygen applied during the normally hypoxic blastema phase prolongs the osteoclast driven bone degradation phase even after the oxygen application has been removed. This fact suggests that increased oxygen not only promotes immediate effects but also cues and sustains a series of cellular changes downstream of the original oxygen application. Although our data imply that our results are the direct consequence of changes in oxygen, our studies do not exclude the fact that these changes may be due to the elevated activity of free oxygen radicals (ROS) generated downstream from hyperoxia [49, 50]. These mechanisms will likely prove to be the focus of future studies.

Prolonged bone degradation after HBOT is in accordance with earlier *in vitro* hyperbaric studies on osteoclast activity that demonstrate increased osteoclast activity [51-55]; however, our findings contrast recent studies showing hypoxic conditions increase the number, size, and activity of osteoclasts [56, 57]. Since osteoclast activity linked to the digit regenerative response is transient and a decline in osteoclast numbers is associated with the

hypoxic blastema [2], it is likely that the role that oxygen plays in osteoclast activity is context dependent. Indeed, the exacerbated degradation we observe during P3 regeneration is not observed in HBOT of uninjured digits, suggesting that the oxygen-related degradation response is dependent upon secondary factors associated with multi-tissue injury.

Our studies show that reducing oxygen during the bone mineralization phase can inhibit bone growth *in vitro* but increasing oxygen with HBOT does not modify the *in vivo* rate of bone growth during regeneration. This finding is consistent with the conclusion that oxygen, or its downstream effects, is required for bone regeneration but is not rate limiting. Similarly, studies *in vitro* have shown that hypoxia limits the bone forming capacity of committed osteoblasts [56, 58-60]. Adequate oxygen levels are known to be required for collagen hydroxylation; pro-collagen molecules that are not effectively hydroxylated are unable to undergo appropriate folding and are retained in the cytoplasm [58, 61]. Once the cell attains critical oxygen levels needed for hydroxylation, collagen excretion proceeds as usual, producing an immediate reaction to increases in oxygen [62]. Thus, hypoxic conditions may temper bone mineralization in a cell-independent manner by inhibiting the hydroxylation of collagen. Nevertheless, our finding that HBOT does not induce precocious bone mineralization suggests that oxygen tension itself is not acting to cue the onset of bone mineralization as the blastema transitions to the re-differentiation phase.

The hypoxic event that we observe prior to blastema formation is largely restricted to the P3 bone marrow and may be associated with the activation of bone marrow derived progenitor cells. Studies characterizing the bone marrow stem cell niche show activated progenitor cells become increasingly hypoxic when stimulated to mobilize [63]. At DPA 7 we see a similar dramatic increase in the number of hypoxic cells in the bone marrow, particularly along the endosteum, and suggest this increase could correspond to progenitor cell activation. Osteoblast progenitor cells have been shown to contribute to digit tip regeneration [64], and *in vitro* studies show that hypoxic micro-environments promote proliferation [65, 66], and delay osteoblastic differentiation [67-73]. These data are consistent with the idea that a bone marrow specific hypoxic event is required for stem cell activation during the digit regenerative response. The recent demonstration that a hypoxic event is linked to cardiomyocyte proliferation during zebrafish heart regeneration is also consistent with this conclusion [74]. Overall, these studies provide strong

evidence that the dynamic regulation of oxygen tension *in vivo* plays a critical role for stem cell activation and blastema formation during a regenerative response.

In summary, the oxygen micro-environment changes dynamically during successful regeneration in mammals. Early events are characterized by a hypoxic bone marrow and may be linked to the activation of progenitor cells. Subsequent hypoxic events in the blastema are associated with the maintenance of proliferation and the transition from a tissue degradation phase to a tissue rebuilding phase. Finally, we show a release from hypoxia is necessary for the re-differentiation of bone tissue. Identifying the anabolic and catabolic effects of oxygen during regeneration underscores the magnitude of the temporal influence of environmental cues. Identifying and exploiting this timeframe for the development of future regeneration therapies will be critical and will hopefully lead to endeavors that will allow us to convey directed, patterned bone regeneration where it does not yet exist. Our studies represent an encouraging step towards refining techniques for alternative therapies for regeneration.

Acknowledgments

Funding was provided by a research grant from the Eunice Kennedy Shriver National Institute of Child Health and Human Development NIH-F32HD071763-02, DARPA-W911NF-06-1-0161, ARO-W911NF0910305, and the John L. and Mary Wright Ebaugh Endowment Fund at Tulane University. The funders had no role in study design, data collection and analysis, decision to publish, or preparation of manuscript. Authors' roles: Conceived and designed the experiments: MS, JS, and KM. Performed the experiments: MS, JS, DF, AC, AW. Analyzed the data: MS, JS, DF, AC, KM. Contributed equipment/materials: KM, KVM. Wrote the paper: MS, JS, KM. Revising manuscript content: All authors. Approving final version: All authors. KM takes responsibility for the integrity of the data analysis.

References

1. Han M, Yang X, Lee J, Allan CH and Muneoka K. Development and regeneration of the neonatal digit tip in mice. *Dev Biol*. 2008; 315: 125-35.
2. Fernando WA, Leininger E, Simkin J, et al. Wound healing and blastema formation in regenerating digit tips of adult mice. *Dev Biol*. 2011; 350: 301-10.
3. Neufeld DA and Zhao W. Bone regrowth after digit tip amputation in mice is equivalent in adults and neonates. *Wound Repair Regen*. 1995; 3: 461-6.
4. Douglas BS. Conservative management of guillotine amputation of the finger in children. *Aust Paediatr J*. 1972; 8: 86-9.
5. Borgens RB. Mice regrow the tips of their foretoes. *Science*. 1982; 217: 747-50.
6. Illingworth CM. Trapped fingers and amputated finger tips in children. *J Pediatr Surg*. 1974; 9: 853-58.
7. Singer M, Weckesser EC, Geraudie J, Maier CE and Singer J. Open finger tip healing and replacement after distal amputation in rhesus monkey with comparison to limb regeneration in lower vertebrates. *Anat Embryol (Berl)*. 1987; 177: 29-36.
8. Muneoka K, Allan CH, Yang X, Lee J and Han M. Mammalian regeneration and regenerative medicine. *Birth Defects Res C Embryo Today*. 2008; 84: 265-80.
9. Rinkevich Y, Lindau P, Ueno H, Longaker MT and Weissman IL. Germ-layer and lineage-restricted stem/progenitors regenerate the mouse digit tip. *Nature*. 2011; 476: 409-13.
10. Takeo M, Chou WC, Sun Q, et al. Wnt activation in nail epithelium couples nail growth to digit regeneration. *Nature*. 2013; 499: 228-32.
11. McKim LH. Regeneration of the Distal Phalanx. *Canadian Medical Association journal*. 1932; 26: 549-50.
12. Vidal P and Dickson MG. Regeneration of the distal phalanx. A case report. *Journal of hand surgery*. 1993; 18: 230-3.
13. Wicker J and Kamler K. Current concepts in limb regeneration: a hand surgeon's perspective. *Ann N Y Acad Sci*. 2009; 1172: 95-109.
14. Bryant SV, Endo T and Gardiner DM. Vertebrate limb regeneration and the origin of limb stem cells. *Int J Dev Biol*. 2002; 46: 887-96.
15. Brockes JP and Kumar A. Appendage regeneration in adult vertebrates and implications for regenerative medicine. *Science*. 2005; 310: 1919-23.
16. Said S, Parke W and Neufeld DA. Vascular supplies differ in regenerating and nonregenerating amputated rodent digits. *Anat Rec A Discov Mol Cell Evol Biol*. 2004; 278: 443-9.
17. Wan C, Shao J, Gilbert SR, et al. Role of HIF-1alpha in skeletal development. *Ann N Y Acad Sci*. 2010; 1192: 322-6.
18. Wang Y, Wan C, Deng L, et al. The hypoxia-inducible factor alpha pathway couples angiogenesis to osteogenesis during skeletal development. *J Clin Invest*. 2007; 117: 1616-26.
19. Love NR, Chen Y, Ishibashi S, et al. Amputation-induced reactive oxygen species are required for successful Xenopus tadpole tail regeneration. *Nat Cell Biol*. 2013; 15: 222-8.
20. Gauron C, Rampon C, Bouzaffour M, et al. Sustained production of ROS triggers compensatory proliferation and is required for regeneration to proceed. *Sci Rep*. 2013; 3: 2084.
21. Jonsson K, Hunt TK and Mathes SJ. Oxygen as an isolated variable influences resistance to infection. *Ann Surg*. 1988; 208: 783-7.
22. Hopf HW, Hunt TK, West JM, et al. Wound tissue oxygen tension predicts the risk of wound infection in surgical patients. *Arch Surg*. 1997; 132: 997-1004.
23. Jonsson K, Jensen JA, Goodson WH, 3rd, et al. Tissue oxygenation, anemia, and perfusion in relation to wound healing in surgical patients. *Ann Surg*. 1991; 214: 605-13.

24. Sen CK and Roy S. Oxygenation state as a driver of myofibroblast differentiation and wound contraction: hypoxia impairs wound closure. *J Invest Dermatol*. 2010; 130: 2701-3.
25. Shweiki D, Itin A, Soffer D and Keshet E. Vascular endothelial growth factor induced by hypoxia may mediate hypoxia-initiated angiogenesis. *Nature*. 1992; 359: 843-5.
26. Allen DB, Maguire JJ, Mahdavian M, et al. Wound hypoxia and acidosis limit neutrophil bacterial killing mechanisms. *Arch Surg*. 1997; 132: 991-6.
27. Gorlach A, Brandes RP, Bassus S, et al. Oxidative stress and expression of p22phox are involved in the up-regulation of tissue factor in vascular smooth muscle cells in response to activated platelets. *FASEB J*. 2000; 14: 1518-28.
28. Gahwiler BH, Capogna M, Debanne D, McKinney RA and Thompson SM. Organotypic slice cultures: a technique has come of age. *Trends Neurosci*. 1997; 20: 471-7.
29. Sloan AJ, Shelton RM, Hann AC, Moxham BJ and Smith AJ. An in vitro approach for the study of dentinogenesis by organ culture of the dentine-pulp complex from rat incisor teeth. *Arch Oral Biol*. 1998; 43: 421-30.
30. McElderry JD, Zhao G, Khmaladze A, Wilson CG, Franceschi RT and Morris MD. Tracking circadian rhythms of bone mineral deposition in murine calvarial organ cultures. *J Bone Miner Res*. 2013; 28: 1846-54.
31. Opperman LA, Passarelli RW, Morgan EP, Reintjes M and Ogle RC. Cranial sutures require tissue interactions with dura mater to resist osseous obliteration in vitro. *J Bone Miner Res*. 1995; 10: 1978-87.
32. Doube M, Klosowski MM, Arganda-Carreras I, et al. BoneJ: Free and extensible bone image analysis in ImageJ. *Bone*. 2010; 47: 1076-9.
33. Karsenty G, Kronenberg HM and Settembre C. Genetic control of bone formation. *Annu Rev Cell Dev Biol*. 2009; 25: 629-48.
34. Jin GY, Li SJ, Moulder JE and Raleigh JA. Dynamic measurements of hexafluoromisonidazole (CCI-103F) retention in mouse tumours by 1H/19F magnetic resonance spectroscopy. *Int J Radiat Biol*. 1990; 58: 1025-34.
35. Raleigh JA, Franko AJ, Treiber EO, Lunt JA and Allen PS. Covalent binding of a fluorinated 2-nitroimidazole to EMT-6 tumors in Balb/C mice: detection by F-19 nuclear magnetic resonance at 2.35 T. *Int J Radiat Oncol Biol Phys*. 1986; 12: 1243-5.
36. Raleigh JA, Franko AJ, Kelly DA, Trimble LA and Allen PS. Development of an in vivo 19F magnetic resonance method for measuring oxygen deficiency in tumors. *Magn Reson Med*. 1991; 22: 451-66.
37. Hausmann A, Lee J and Pantopoulos K. Redox control of iron regulatory protein 2 stability. *FEBS Lett*. 2011; 585: 687-92.
38. Recalcati S, Minotti G and Cairo G. Iron regulatory proteins: from molecular mechanisms to drug development. *Antioxid Redox Signal*. 2010; 13: 1593-616.
39. Ruiz JC, Walker SD, Anderson SA, Eisenstein RS and Bruick RK. F-box and leucine-rich repeat protein 5 (FBXL5) is required for maintenance of cellular and systemic iron homeostasis. *J Biol Chem*. 2013; 288: 552-60.
40. Forsythe JA, Jiang BH, Iyer NV, et al. Activation of vascular endothelial growth factor gene transcription by hypoxia-inducible factor 1. *Mol Cell Biol*. 1996; 16: 4604-13.
41. Chollangi S, Thompson JW, Ruiz JC, Gardner KH and Bruick RK. Hemerythrin-like domain within F-box and leucine-rich repeat protein 5 (FBXL5) communicates cellular iron and oxygen availability by distinct mechanisms. *J Biol Chem*. 2012; 287: 23710-7.
42. Vashisht AA, Zumbrennen KB, Huang X, et al. Control of iron homeostasis by an iron-regulated ubiquitin ligase. *Science*. 2009; 326: 718-21.
43. Salahudeen AA, Thompson JW, Ruiz JC, et al. An E3 ligase possessing an iron-responsive hemerythrin domain is a regulator of iron homeostasis. *Science*. 2009; 326: 722-6.
44. Modak SP and Perdue SW. Terminal lens cell differentiation. I. Histological and microspectrophotometric analysis of nuclear degeneration. *Exp Cell Res*. 1970; 59: 43-56.

45. Gavrieli Y, Sherman Y and Ben-Sasson SA. Identification of programmed cell death in situ via specific labeling of nuclear DNA fragmentation. *J Cell Biol*. 1992; 119: 493-501.
46. Garrity MM, Burgart LJ, Riehle DL, Hill EM, Sebo TJ and Witzig T. Identifying and quantifying apoptosis: navigating technical pitfalls. *Mod Pathol*. 2003; 16: 389-94.
47. Eliasson P and Jonsson JI. The hematopoietic stem cell niche: low in oxygen but a nice place to be. *J Cell Physiol*. 2010; 222: 17-22.
48. Albert M. The Role of Hyperbaric Oxygen Therapy in Wound Healing. *Wound Care Canada*. 2008; 6: 60-2.
49. Narkowicz CK, Vial JH and McCartney PW. Hyperbaric oxygen therapy increases free radical levels in the blood of humans. *Free radical research communications*. 1993; 19: 71-80.
50. Sjoberg F and Singer M. The medical use of oxygen: a time for critical reappraisal. *Journal of internal medicine*. 2013; 274: 505-28.
51. Gray DH, Katz JM and Speak K. The effects of varying oxygen tensions upon bone resorption in vitro. *J Bone Joint Surg Br*. 1978; 60-B: 575-8.
52. Goldhaber P. The effect of hyperoxia on bone resorption in tissue culture. *AMA Arch Pathol*. 1958; 66: 635-41.
53. Stern B, Glimacher MJ and Goldhaber P. The effect of various oxygen tensions on the synthesis and degradation of bone collagen in tissue culture. *Proc Soc Exp Biol Med*. 1966; 121: 869-72.
54. Shaw JL and Bassett CA. The effects of varying oxygen concentrations on osteogenesis and embryonic cartilage in vitro. *J Bone Joint Surg Am*. 1967; 49: 73-80.
55. Brighton CT and Schaffzin EA. Comparison of the effects of excess vitamin A and high oxygen tension on in vitro epiphyseal plate growth. I. Morphologic response. *Calcif Tissue Res*. 1970; 6: 151-61.
56. Arnett TR. Acidosis, hypoxia and bone. *Arch Biochem Biophys*. 2010; 503: 103-9.
57. Arnett TR, Gibbons DC, Utting JC, et al. Hypoxia is a major stimulator of osteoclast formation and bone resorption. *J Cell Physiol*. 2003; 196: 2-8.
58. Utting JC, Robins SP, Brandao-Burch A, Orriss IR, Behar J and Arnett TR. Hypoxia inhibits the growth, differentiation and bone-forming capacity of rat osteoblasts. *Exp Cell Res*. 2006; 312: 1693-702.
59. Araldi E and Schipani E. Hypoxia, HIFs and bone development. *Bone*. 2010; 47: 190-6.
60. Wang Y, Wan C, Gilbert SR and Clemens TL. Oxygen sensing and osteogenesis. *Ann N Y Acad Sci*. 2007; 1117: 1-11.
61. Fessler LI and Fessler JH. Protein assembly of procollagen and effects of hydroxylation. *J Biol Chem*. 1974; 249: 7637-46.
62. Ramaley PB and Rosenbloom J. Inhibition of proline and lysine hydroxylation prevents normal extrusion of collagen by 3T6 fibroblasts in culture. *FEBS Lett*. 1971; 15: 59-64.
63. Levesque JP, Winkler IG, Hendy J, et al. Hematopoietic progenitor cell mobilization results in hypoxia with increased hypoxia-inducible transcription factor-1 alpha and vascular endothelial growth factor A in bone marrow. *Stem Cells*. 2007; 25: 1954-65.
64. Lehoczky JA, Robert B and Tabin CJ. Mouse digit tip regeneration is mediated by fate-restricted progenitor cells. *Proc Natl Acad Sci U S A*. 2011; 108: 20609-14.
65. Tuncay OC, Ho D and Barker MK. Oxygen tension regulates osteoblast function. *Am J Orthod Dentofacial Orthop*. 1994; 105: 457-63.
66. Matsuda N, Morita N, Matsuda K and Watanabe M. Proliferation and differentiation of human osteoblastic cells associated with differential activation of MAP kinases in response to epidermal growth factor, hypoxia, and mechanical stress in vitro. *Biochem Biophys Res Commun*. 1998; 249: 350-4.
67. Ontiveros C, Irwin R, Wiseman RW and McCabe LR. Hypoxia suppresses runx2 independent of modeled microgravity. *J Cell Physiol*. 2004; 200: 169-76.
68. Park JH, Park BH, Kim HK, Park TS and Baek HS. Hypoxia decreases Runx2/Cbfa1 expression in human osteoblast-like cells. *Mol Cell Endocrinol*. 2002; 192: 197-203.
69. Salim A, Nacamuli RP, Morgan EF, Giaccia AJ and Longaker MT. Transient changes in oxygen tension inhibit osteogenic differentiation and Runx2 expression in osteoblasts. *J Biol Chem*. 2004; 279: 40007-16.

70. Yang DC, Yang MH, Tsai CC, Huang TF, Chen YH and Hung SC. Hypoxia Inhibits Osteogenesis in Human Mesenchymal Stem Cells through Direct Regulation of RUNX2 by TWIST. *PLoS ONE*. 2011; 6: e23965.
71. Csete M. Oxygen in the cultivation of stem cells. *Ann N Y Acad Sci*. 2005; 1049: 1-8.
72. Das R, Jahr H, van Osch GJ and Farrell E. The role of hypoxia in bone marrow-derived mesenchymal stem cells: considerations for regenerative medicine approaches. *Tissue Eng Part B Rev*. 2010; 16: 159-68.
73. Zahm AM, Bucaro MA, Srinivas V, Shapiro IM and Adams CS. Oxygen tension regulates preosteocyte maturation and mineralization. *Bone*. 2008; 43: 25-31.
74. Jopling C, Sune G, Faucherre A, Fabregat C and Izpisua Belmonte JC. Hypoxia induces myocardial regeneration in zebrafish. *Circulation*. 2012; 126: 3017-27.
75. Dempster DW, Compston JE, Drezner MK, et al. Standardized nomenclature, symbols, and units for bone histomorphometry: a 2012 update of the report of the ASBMR Histomorphometry Nomenclature Committee. *J Bone Miner Res*. 2013; 28: 2-17.

Fig. 1. In vivo bone regeneration shows distinct phases of degradation and growth. (A) Bone regeneration shows an initial phase of bone degradation before beginning to grow bone at DPA 10 (N=5 mice, N=10 digits). Samples were analyzed for bone growth using μCT. Data is normalized to initial DPA 0 bone volume. Error bars represent SEM. (B) Representative sample of μCT-generated 3D renderings of the P3 regeneration timeline in vivo are shown beneath the X-axis.

Fig. 2. P3 regeneration represents a dynamic oxygen microenvironment. (A-H) Oxygen profiling in vivo using Hypoxyprobe-1 (<1.3% oxygen) indicates hypoxic micro-environments (<1.3% oxygen) at DPA 7 (marrow), 12 (blastema), and 14 (trabecular spaces). (E) Arrow indicates hypoxic signal at the distal edge of the bone stump. (A'-H') Positive signal from oxygen-stabilized protein FBXL5 (>5%-6% oxygen) shows signal in the marrow in the unamputated and DPA 0-10. FBXL5 is also apparent at DPA 3-12 in the dorsal proximal connective tissue N=3, representative sample shown. (I-K) Colorimetric overlay of hypoxyprobe (pink) and FBXL5 (green) as compared to normoxic (purple) areas at DPA 10, 12, and 14. (L) The anti-hypoxyprobe (pink) and anti-FBXL5 (green) stained cells were selected and plotted as cell counts versus DAPI staining. Percentages of cells are shown in the bar graph. Cells expressing DAPI signal only are shown as the remaining percentage (purple). Scale bar represents 100 μm. N=4 with representative sample shown. Distal = left, proximal = right

Fig. 3. **Slice culture models regenerate bone *ex vivo*.** Digits were removed at DPA 7 (A), 11 (B), and 14 (C), and slices were grown in culture for 7 days (D-F). Whole mount Alizarin red staining shows bone regression and growth at different time points along the regeneration timeline (arrow). DPA 11 and DPA 14 samples show new bone growth (dotted black) when compared to the estimated original bone (solid white). Initial time depicts digits at time of removal. 7 days in culture shows slices after 7 days post slice. Regeneration after 7 days in vivo is included for comparison (G-I). Original bone prior to degradation is shown outlined in solid black. Sequential labeling of regenerating bone was performed *in vivo* using calcein green and subsequently *ex vivo* using alizarin complexone (J-K). *Ex vivo* bone regeneration, shown in red, is evident at the progressing perimeter of the original calcein labeled bone (J, arrow). Areas of *ex vivo* bone growth that are independent of calcein staining are also

apparent at the distal end of P3 (J, asterisk) 100x magnification. At 400x magnification, areas of Alizarin-positive bone are associated with osterix-positive cells (K, asterix) and areas of calcien-positive bone are associated with osterix-negative cells (K, arrow). Green= Calcien, Red= Alizarin Red Complexone, Pink = Osterix, Grey= DAPI N=2 (*in vivo*), N=3 (slice) with representative sample shown.

Fig. 4. **The anabolic effect of oxygen is temporally specific during P3 regeneration.** (A) DPA 14 explant slice samples show a distinct pattern of new bone formation in culture. Overlaid μCT-generated 3D renderings of a representative slice sample show areas of new bone growth (DPS 14) in red, and original bone (DPS 0) in gray. (B) Micro-CT scans of the same sample seen in 4A are pseudo-colored according to trabecular thickness. Color changes indicate bone thickness in mm with an example of increasing thickness across time points indicated by the arrow. Sample cross-sections show a distinct marrow cavity throughout culture. (C) DPA 14 slice samples fail to mineralize bone at 1% oxygen (N=5), but show bone growth at 21% oxygen (N=8). (D) In contrast, DPA 12 slice samples fail to mineralize bone at 21% oxygen (N=5), but show an increase in bone after culture at 1% oxygen tension (N=4)

Fig. 5. **Disruption of the blastema hypoxic event prevents optimal P3 regeneration**. (A) DPA 12 hypoxic blastema prior to HBOT treatment (B) DPA 12 blastema 5 hours after HBOT treatment shows no hypoxic signal. Scale bar = 100 μm (C-D) Tracking the bone volume changes of individual digits during the regeneration process reveals two groups of mice. In the first group (C), bone degradation ends and bone growth begins between DPA 7 and DPA 10 (n=21 digits). In the second group bone degradation ends and bone regeneration begins between DPA 10 and 14 (D, n=11 digits). Black bars show inclusive area of bone volume turn-around. (E-F) Mice treated with HBOT at DPA 11 and DPA 13 respond differently to treatment depending upon the stage of regeneration. Digits treated with HBOT after bone regeneration has already begun (E, n=13), show little response to hyperbaric treatment and graphs appear similar to control digits (C). Digits treated with HBOT prior to the bone growth phase (F, n=19) show a prolonged period of degradation and a wider range of bone degradation to bone growth turn-around points (black bar). (G) Time lapse imaging showing the P3 regenerative response in a control digit. (H)

Time lapse imaging of a representative digit (from F) treated with HBOT at DPA 11 and DPA 13 showing prolonged bone degradation and a slower rate of bone growth.

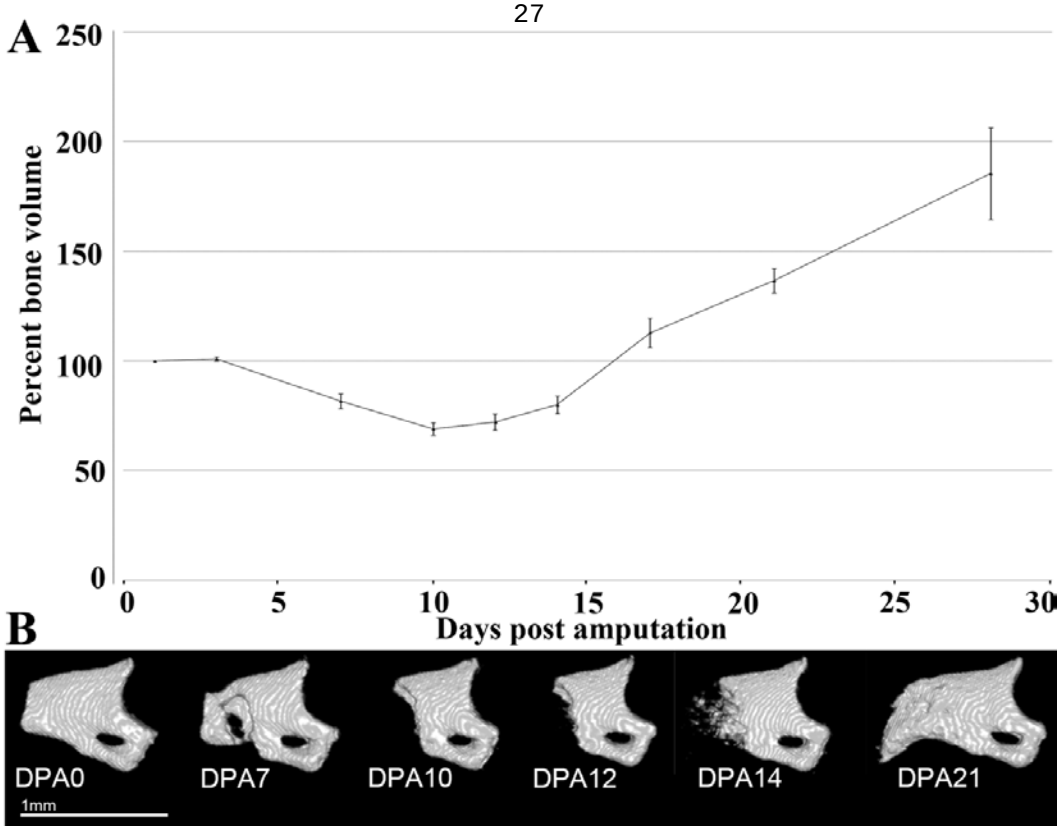

Figure 1

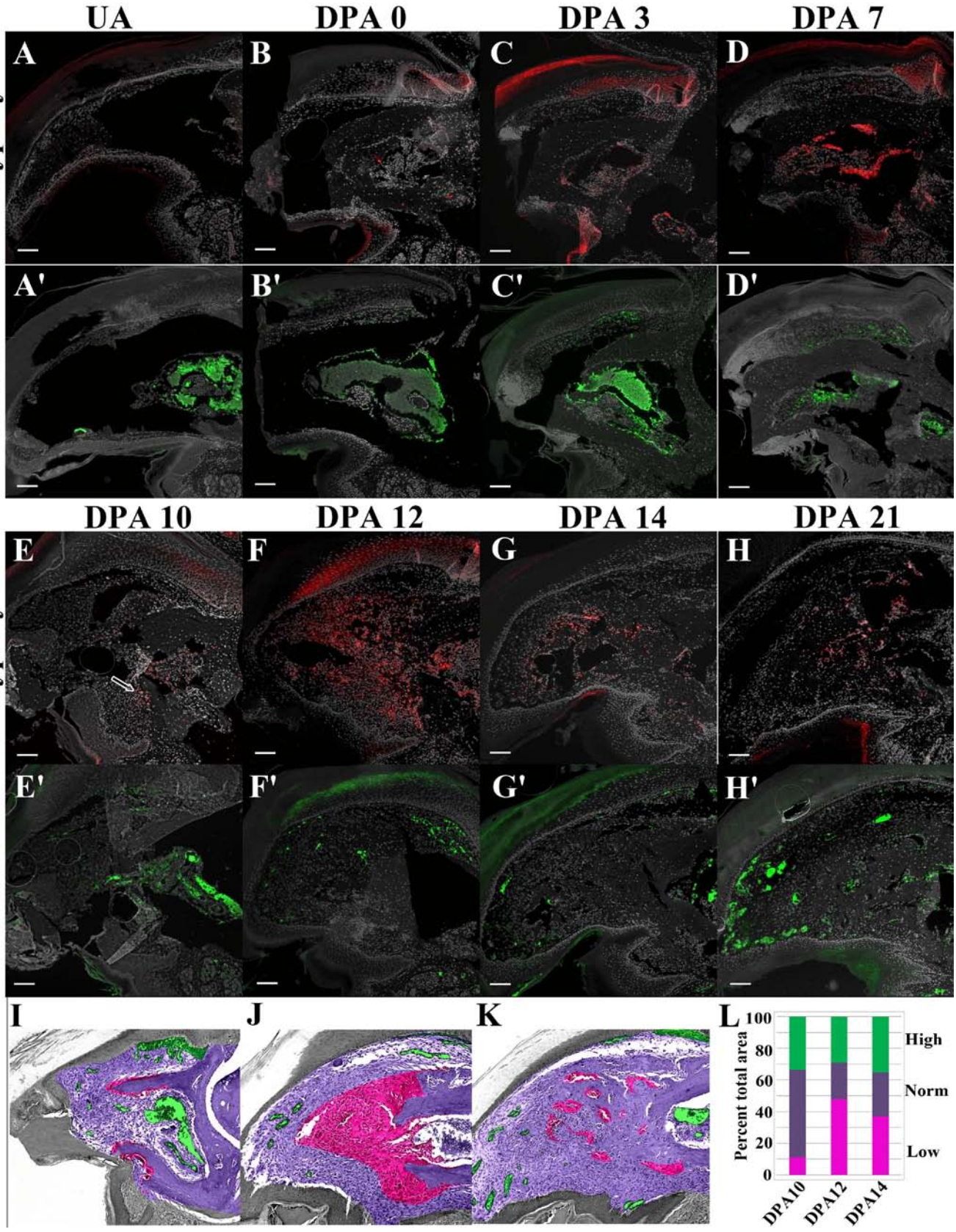

Figure 2

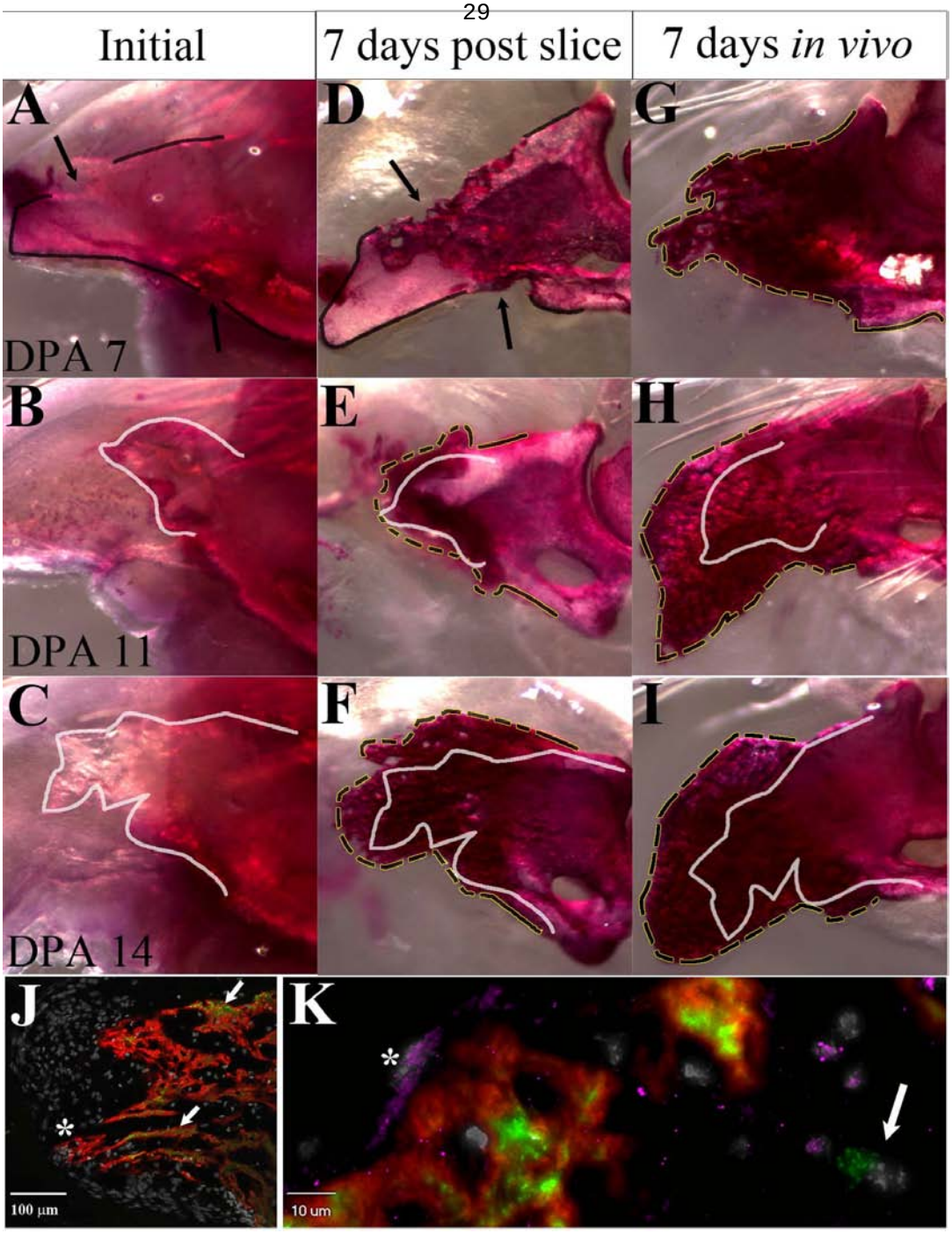

Figure 3

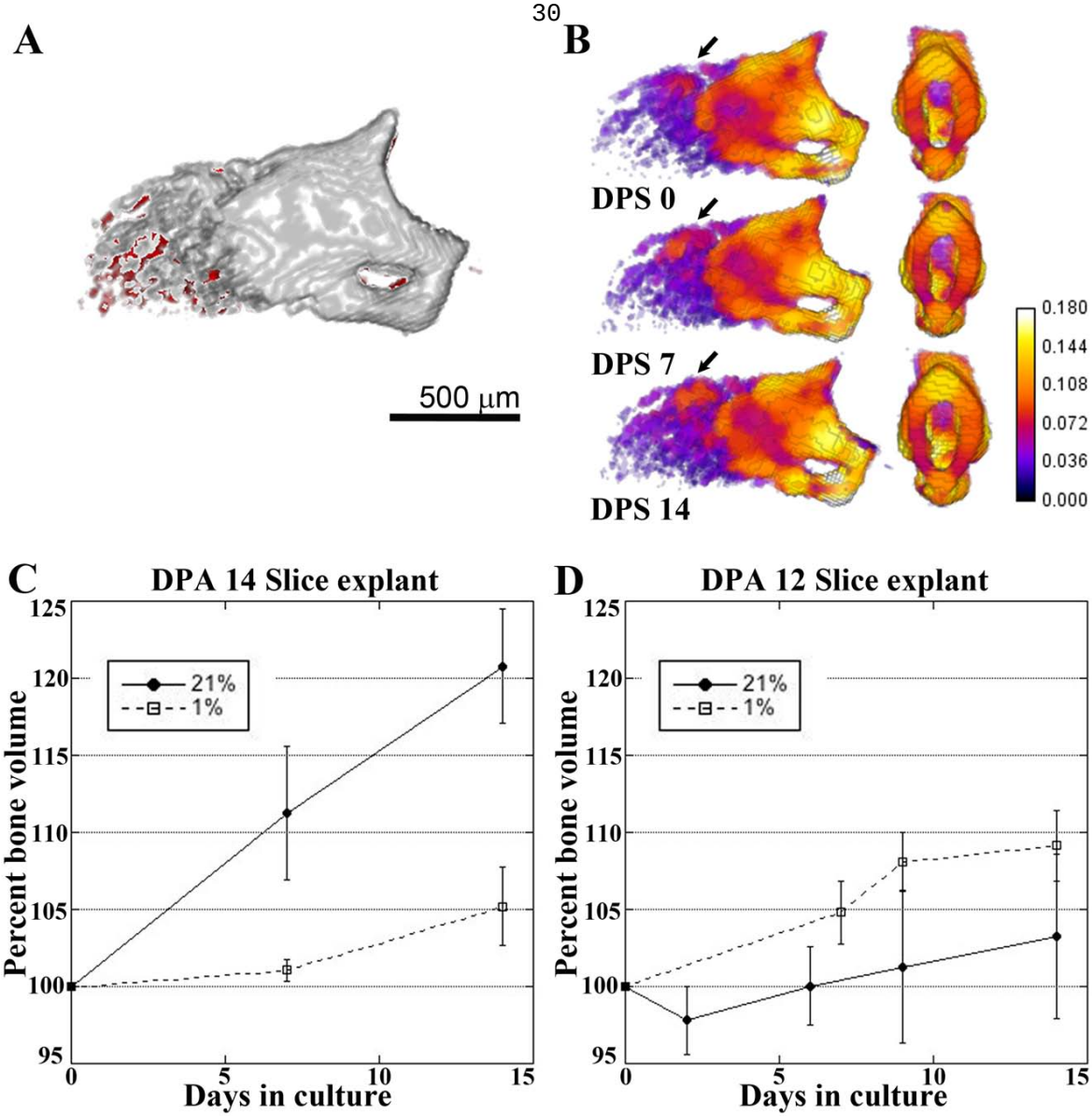

Figure 4

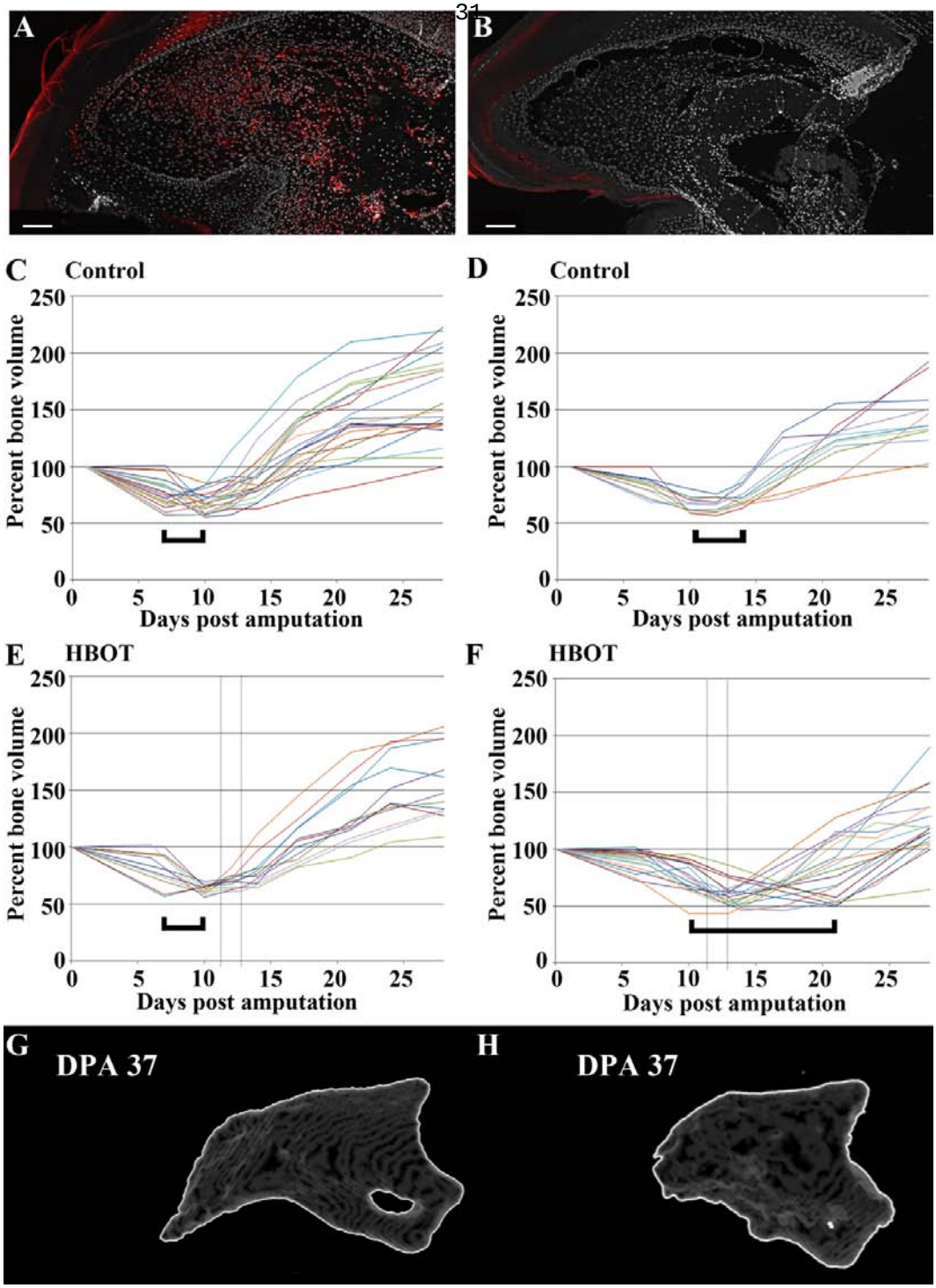

Figure 5